Electronic Supplementary Information (ESI) for the manuscript:

Electroswitching of the single-molecule magnet behaviour in an octahedral spin crossover cobalt(II) complex with a redox-active pyridinediimine ligand

Renato Rabelo, Luminita Toma,* Nicolás Moliner, Miguel Julve, Francesc Lloret, Jorge Pasán, Catalina Ruiz-Pérez, Rafael Ruiz-García and Joan Cano*

Table of Contents

Materials

Reagent grade pyridine-2,6-diformaldehyde, 4-anisidine, acetic acid, bromine, hydrazine, and cobalt(II) perchlorate hexahydrate were purchased from commercial sources and used as received.

Preparation of the ligand and complexes

4-MeOPhPDI: A mixture of pyridine-2,6-diformaldehyde (0.135 g, 1.0 mmol) and 4-anisidine (0.246 g, 2.0 mmol) in 5.0 mL of ethanol plus 100 μL of acetic acid were allowed to reflux for 30 min. A brown crystalline solid separates when the mixture was cooled in an ice bath. It was collected by filtration and washed with a small amount of ethanol. Yield 88%. Anal. Calc. for $C_{21}H_{19}N_3O_2$ (4-MeOPhPDI): C, 73.03; H, 5.54; N, 12.17. Found: C, 73.94; H, 5.13; N, 12.29%. IR (KBr, cm^{-1}): 2965w [ν(C–H) from the methoxy substituents of 4-MeOPhPDI], 1624m [ν(C=N) from the imine groups of 4-MeOPhPDI], 1245s [ν(C–O) from the methoxy substituents of 4-MeOPhPDI]. ^{1}H NMR ($CDCl_3$; 300 MHz, ppm): δ = 8.70 (s, 2H, H_{im}), 8.24 (d, 2H, *m*-H_{py}, J = 7.8 Hz), 7.90 (t, 1H, *p*-H_{py}, J = 7.8 Hz), 7.36 (d, 4H, *o*-H_{ph}, J = 8.9 Hz), 6.96 (d, 4H, *m*-H_{ph}, J = 8.9 Hz), 3.85 (s, 6H, *p*-H_{OMe}).

$[Co(4\text{-}MeOPhPDI)_2](ClO_4)_2$ (**1**): An ethanolic solution (2.0 mL) of cobalt(II) perchlorate hexahydrate (0.035 g, 0.10 mmol) was added dropwise to a suspension of 4-MeOPhPDI (0.070 g, 0.20 mmol) in ethanol (20.0 mL) under stirring. The mixture was further stirred for two hours under gentle warming. The resulting polycrystalline powder was filtered off and washed with a small amount of ethanol. X-ray quality dark red crystals of **1** were obtained by slow diffusion of ethyl acetate into a saturated 1:1 acetonitrile/chloroform solution mixture of the polycrystalline product in a glass tube. Yield 87%. Anal. Calc. for $C_{41}H_{35}N_6O_{12}Cl_2Co$ (**1**): C, 53.18; H, 4.04; N, 8.86. Found:

C, 53.98; H, 4.17; N, 8.90%. IR (KBr, cm^{-1}): 2973m [ν(C–H) from the methoxy substituents of 4-MeOPhPDI], 1596s [ν(C=N) from the imine groups of 4-MeOPhPDI], 1082vs [ν(Cl–O) from perchlorate anion].

$Co(4\text{-}MeOPhPDI)_2](Br_3)_{2.35}(Br_5)_{0.65}\cdot 1/4H_2O$ (**2**): An excess of molecular bromine (75 μL, 0.150 mmol) was added to a 1:1 acetonitrile/chloroform solution mixture of **1** (0.014 g, 0.015 mmol). X-ray suitable dark brown crystals of **2** were obtained by slow diffusion of ethyl acetate into the resulting dark brown solution in a glass tube. They were filtered off and stored in a refrigerator at 4 ºC to prevent for slow thermal decomposition at room temperature. Yield: 78%. Anal. Calc. for $C_{41}H_{35.5}N_6O_{4.25}Br_{10.3}Co$ (**2**): C, 31.52; H, 2.29; N, 5.38. Found: C, 31.55; H, 2.40; N, 5.70%. IR (KBr, cm^{-1}): 2974m [ν(C–H) from the methoxy substituents of 4-MeOPhPDI], 1593s [ν(C=N) from the imine groups of 4-MeOPhPDI].

Physical techniques

Elemental (C, H, N) analyses were performed at the Servicio Central de Soporte a la Investigación (SCSIE) at the Universitat de València (Spain). FT–IR spectra were recorded on a Nicolet-5700 spectrophotometer as KBr pellets. ^1H NMR spectra were registered at room temperature on a Bruker AC 300 (300 MHz) spectrometer. Deuterated chloroform was used as solvent and internal standard (δ = 7.26 ppm). X-ray powder diffraction (XRPD) patterns of powdered crystalline samples were collected at room temperature on a D8 Avance A25 Bruker diffractometer by using graphite-monochromated Cu-Kα radiation (λ = 1.54056 Å).

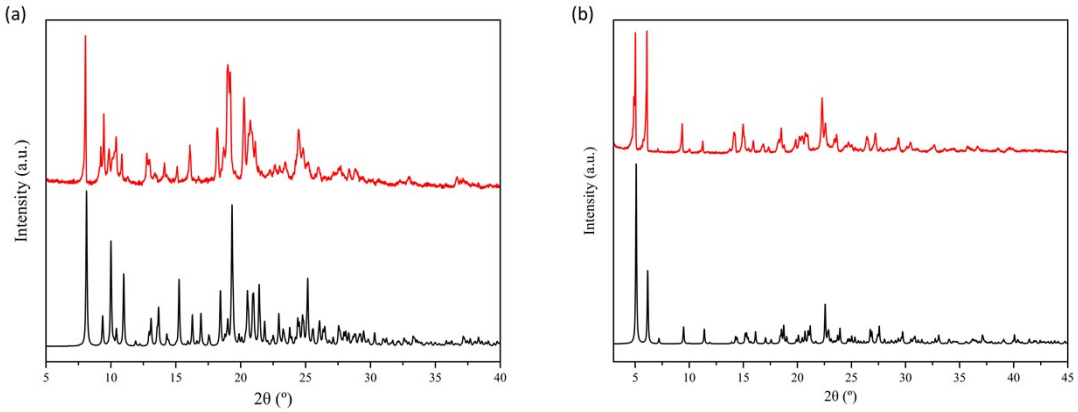

Fig. S1 Experimental XRPD pattern (red line) of **1** (a) and **2** (b) compared to the calculated one (black line).

X-ray crystallographic data collection and structure refinement

X-ray diffraction data on a single crystal of **1** were collected on an Agilent Supernova diffractometer equipped with an EosS2 detector with Mo-Kα radiation (λ = 0.71073 Å) at 150 K, while those of **2** were collected on a Bruker D8 Venture diffractometer with a PHOTON II detector by using monochromatic Mo-Kα radiation (λ = 0.71073 Å) at 120 K. Diffraction data of **1** and **2** were collected, scaled, and integrated using the CrysAlisPro software[1] for **1** and Bruker SAINT[2] for **2**. The structures were solved by intrinsic phasing methods integrated into the SHELXTL software[3] with the Olex2 platform.[4] The obtained models were refined with the version 2018/3 of SHELXL against F^2 on all data by full-matrix least squares. All non-hydrogen atoms were refined anisotropically. Hydrogen atoms, except those of the water molecules, which were neither found nor fixed, were set on geometrical positions and refined with a riding model. The crystals of **2** poorly diffract, most likely because of the disorder of the polybromide anions, and they readily decompose. The crystallographic data presented herein correspond to our best attempt to measure **2** at 120 K, but with the resolution cut at 1.0 Å, as a consequence of not very good completeness. Also, the crystals of **2** decompose with time, and some meaningless electron density peaks appear in the Fourier integration, in particular a maximum residual peak of 2.58 e Å^{-3} which is very close to a phenyl ring.

The X-ray structures **1** and **2** were refined as inversion twins, given the non-centrosymmetry of the space groups, introducing the TWIN/BASF instruction with values of the Flack parameter of 0.210(12) and 0.07(3) for **1** and **2**, respectively. The

[1] Agilent (2014). *CrysAlis PRO*. Agilent Technologies Ltd, Yarnton, Oxfordshire, England.
[2] Bruker (2012). *SAINT*. Bruker AXS Inc., Madison, Wisconsin, USA.
[3] G. M. Sheldrick, *Acta Cryst. A*, 2015, **71**, 3-8.
[4] O. V. Dolomanov, L. J. Bourhis, R. J, Gildea, J. A. K. Howard and H. Puschmann, *J. Appl. Cryst*., 2009, **42**, 339-341.

methyl group of one of the 4-methoxyphenyl-substituted pyridinediimine ligands in **2** is disordered between two positions, and some restraints were applied to the anisotropic displacements of the C atoms. However, the s.o.f. could be refined. One of the Br_3^- and the Br_5^- anions in **2** were disordered. The occupation factor was refined in preliminary steps. Once converged, s.o.f. was fixed to the values 0.35 and 0.65 for the Br_3^- and Br_5^- polyhalide anions. The graphical manipulations and calculations were performed with the CRYSTALMAKER and MERCURY programs.[5,6] Crystallographic data (excluding structure factors) for the structures reported in this paper have been deposited with the Cambridge Crystallographic Data Centre as supplementary publication numbers CCDC–1989325 (**1**) and CCDC–1989324 (**2**). Copies of the data can be obtained free of charge on application to CCDC, 12 Union Road, Cambridge CB21EZ, UK (fax: (+44) 1223−336−033; e-mail: deposit@ccdc.cam.ac.uk).

[5] *CrystalMaker*, CrystalMaker Software, Bicester, England, 2015.
[6] *Mercury*, The Cambridge Crystallographic Data Centre, Cambridge, UK.

Table S1. Summary of Crystallographic Data for **1** and **2**

	1	**2**
Formula	$C_{41}H_{35}N_6O_{12}Cl_2Co$	$C_{42}H_{38}N_6O_{4.25}Br_{9.7}Co$
M (g mol^{-1})	948.61	1546.80
Crystal system	Tetragonal	Tetragonal
Space group	$P4_3$	I-42m
a (Å)	19.3426(1)	24.552(5)
b (Å)	19.3426(1)	24.552(5)
c (Å)	43.5392(5)	17.693(4)
α (°)	90	90
β (°)	90	90
γ (°)	90	90
V (Å^3)	16289.6(3)	10665(5)
Z	16	8
ρ_{calc} (g cm^{-3})	1.547	1.964
μ (mm^{-1})	0.627	8.084
T (K)	150	120
Reflect. collcd.	88667	43052
Reflect. obs. [$I > 2\sigma(I)$]	30594	3616
Data/restraints/parameters	36206/1/2286	3798/8/324
R_1[a] [$I > 2\sigma(I)$]	0.0505 (0.0654)	0.0468 (0.0490)
wR_2[b] [$I > 2\sigma(I)$]	0.1135 (0.1236)	0.1273 0.1290)
S[c]	0.978	1.098

[a] $R_1 = \sum(|F_o| - |F_c|)/\sum|F_o|$. [b] $wR_2 = [\sum w(F_o^2 - F_c^2)^2/\sum w(F_o^2)^2]^{1/2}$. [c] $S = [\sum w(|F_o| - |F_c|)^2/(N_o - N_p)]^{1/2}$.

Table S2. Selected Structural Data for **1** and **2**

	Co1[a]	Co2[a]	Co3[a]	Co4[a]	Co1[b]
R_1(Co–N_{im})[c] (Å)	2.085(4)	2.180(4)	2.090(4)	2.185(4)	1.979(10)
R_2(Co–N'$_{im}$)[c] (Å)	2.085(4)	2.114(4)	2.076(4)	2.096(4)	1.979(10)
R_3(Co–N_{py})[d] (Å)	1.872(5)	1.905(5)	1.874(5)	1.902(5)	1.842(9)
R_{eq}[e] (Å)	2.085(4)	2.147(4)	2.083(4)	2.141(4)	1.979(10)
δ_R[f]	0	0.031	0.007	0.042	0
R[g] (Å)	2.014(5)	2.066(5)	2.013(5)	2.061(5)	1.933(10)
Δ_R[h]	0.106(5)	0.117(5)	0.103(5)	0.115(5)	0.071(9)
N_{im}–Co–N'$_{im}$[i] (º)	84.1(2)	92.0(2)	84.2(2)	92.1(2)	85.6(4)
N'$_{im}$–Co–N_{im}[i] (º)	100.1(2)	92.6(2)	100.0(2)	92.4(2)	96.5(6)
N_{py}–Co–N_{py}[j] (º)	177.4(2)	176.6(2)	178.4(2)	178.5(2)	175.1(6)
δ[k] (Å)	±0.395	±0.430	±0.395	±0.421	±0.295
Φ[l] (º)	72.2(2)	89.9(2)	72.7(2)	89.9(2)	80.8(6)
ϕ[m] (º)	43.7(8)	41.3(8)	44.5(8)	40.5(8)	47.5(6)
h[n] (Å)	3.839(4)	4.273(4)	3.939(4)	4.502(4)	3.905(9)
θ[o] (º)	23.5(2)	30.3(2)	23.4(2)	20.7(3)	22.9(6)

[a]Structural data for each of the four crystallographically independent cobalt atoms of **1**. [b]Structural data for the unique crystallographically independent cobalt atom of **2**. [c]Average cobalt to imine-nitrogen equatorial bond distances from each ligand. [d]Mean cobalt to pyridine-nitrogen axial bond distances from the two ligands. [e]Average cobalt to equatorial nitrogen bond distances defined as $R_{eq} = (R_1 + R_2)/2$. [f]Rhombic distortion parameter defined as $\delta_R = (R_1 - R_2)/R_{eq}$. [g]Mean cobalt-nitrogen bond distances defined as $R = (R_1 + R_2 + R_3)/3$. [h]Axial distortion parameter defined as $\Delta_R = (R_{eq} - R_{ax})/R$. [i]Average cobalt to imine-nitrogen equatorial bond angles from the two ligands. [j]Average cobalt to pyridine-nitrogen axial bond angles from the two ligands. [k]Mean deviations of the imine-nitrogen donor atoms from the metal equatorial plane. [l]Dihedral angle between the mean planes of the pyridinediimine ligand fragments. [m]Average torsional angle for the phenylimine ligand fragments. [n]Intramolecular distance between the centroids of the pyridine and phenyl rings from the two ligands. [o]Offset dihedral angle between the normal of pyridine and phenyl mean planes respect to the centroid···centroid vector.

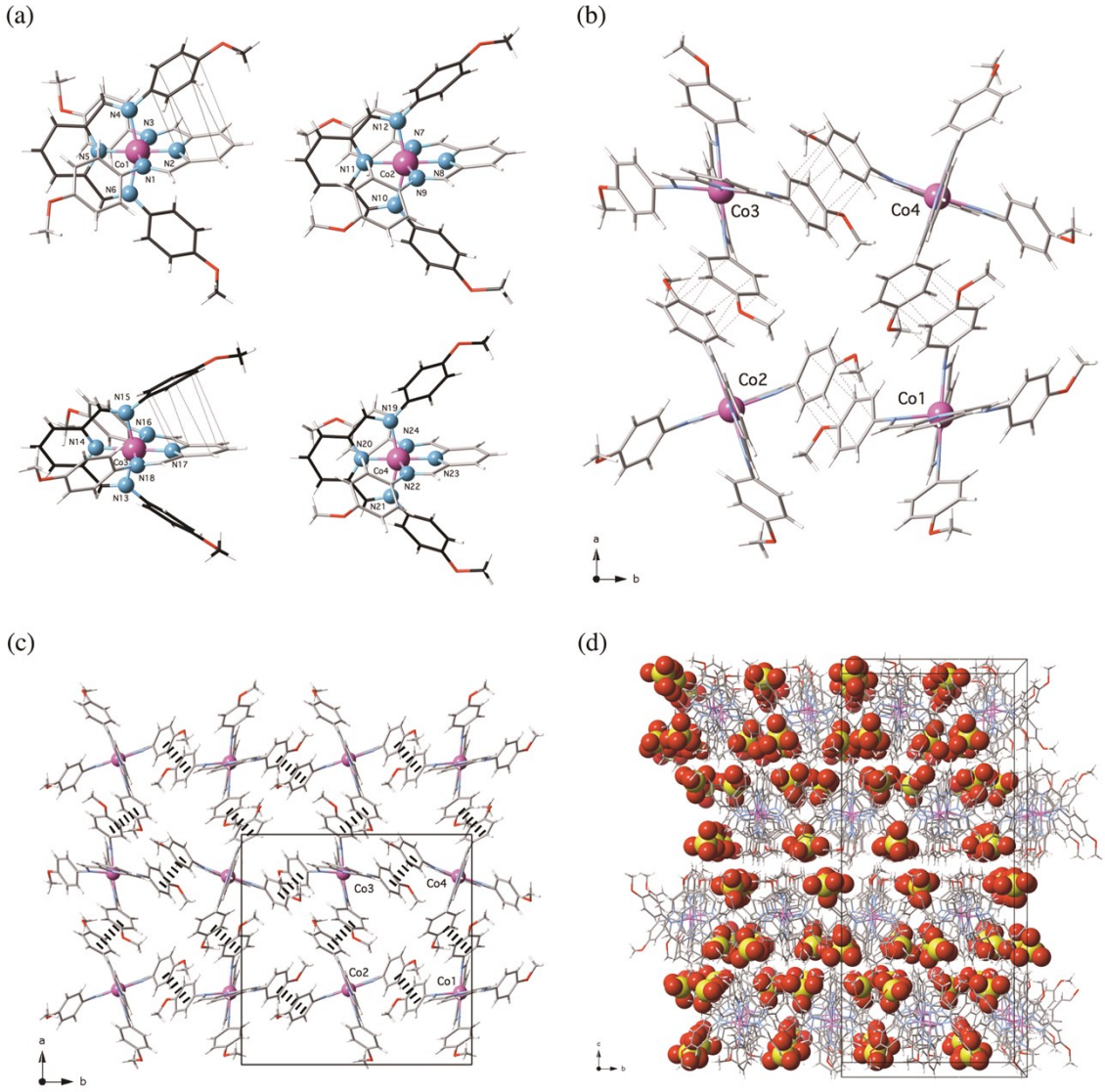

Fig. S2 (a) Perspective views of the four crystallographically independent cationic mononuclear cobalt(II) units of **1** with the atom numbering scheme for the first coordination sphere of the metal atoms (each of the two ligand backbones are drawn in light and dark grey black colours for clarity). The intramolecular π-π stacking interactions are drawn as dotted lines. (b) View of the π-bonded square motif of the cationic mononuclear cobalt(II) units of **1** along the [001] direction. The intermolecular π-π stacking interactions are drawn as dotted lines. (c) Projection of a layer of the cationic mononuclear cobalt(II) units in **1** along the [001] direction showing the array of π-bonded square grids [symmetry codes: (I) = *–x*, *–y*, *–z*; (II) = 1/2*–x*, 1/2+*y*, 1/2*–z*; (III) = 1/2+*x*, 1/2*–y*, 1/2+*z*]. The intermolecular π-π stacking interactions are drawn as dashed lines. (d) View of the crystal packing of **1** along the [100] direction. The perchlorate anions are shown in a space filling representation.

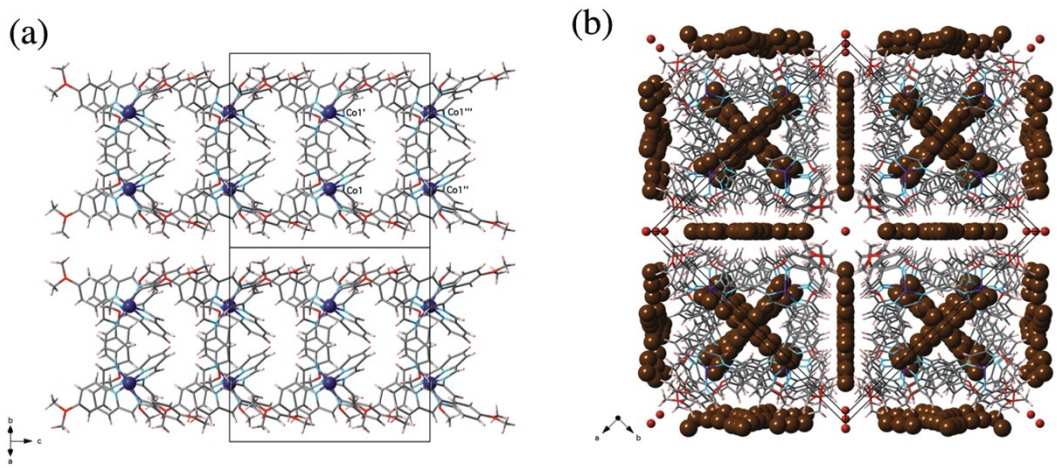

Fig. S3 (a) Projection of a column of pairs of cationic mononuclear cobalt(III) units in **2** along the [001] direction [symmetry codes: (I) = -x, –1–y, z; (II) = –1/2-y, –1/2+x, ½–z; (III) = 1/2+y, –1/2–x, ½–z]. (b) View of the crystal packing of **2** along the [001] direction. The tribromide anions are shown in a space filling representation.

Electrochemical measurements

Cyclic voltammetry and high current electrolysis were performed using an AUTOLAB 204 and booster (Module BOOSTER10A) potentiostat/galvanostat. Cyclic voltammograms were carried out at room temperature using 0.1 M nBu$_4$NPF$_6$ as supporting electrolyte and 1.0 mM of **1** in acetonitrile. The working electrode was a glassy carbon disk (0.32 cm^2) that was polished with 1.0 μm diamond powder, sonicated, washed with absolute ethanol and acetone, and air dried. The reference electrode was AgCl/Ag separated from the test solution by a salt bridge containing the solvent/supporting electrolyte, with platinum as auxiliary electrode. All experiments were performed in standard electrochemical cells under argon. The investigated scan rate and potential *vs*. AgCl/Ag ranges were 20 to 250 mV s^{-1} and –2.0 to +2.0 V, respectively. Ferrocene (Fc) was added as internal standard at the end of the measurements. The formal potentials were measured at a scan rate of 200 mV s^{-1} and they were referred to the Fc$^+$/Fc couple. The values of the measured formal potential and the anodic to cathodic peaks separation of ferrocene under the same conditions are E(Fc$^+$/Fc) = +0.40 V *vs*. AgCl/Ag and ΔE_p(Fc$^+$/Fc) = 80 mV (CH$_3$CN, 0.1 M nBu$_4$NPF$_6$, 25 °C). Electrolysis were successively performed at 0 °C on concentrated 15 mM acetonitrile solutions of **1** at fixed oxidation (E_{ox} = +1 V) and reduction potentials (E_{red} = 0 V) using 0.1 M nBu$_4$NPF$_6$ as supporting electrolyte.

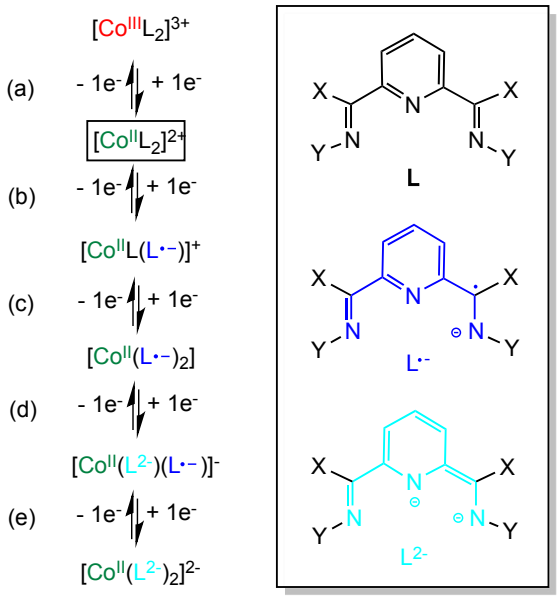

Scheme S1 Proposed redox model for the multielectron transfer series of **1**.

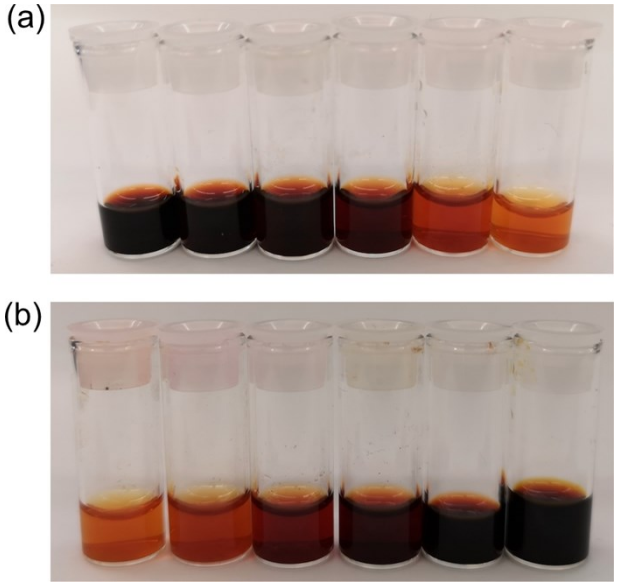

Fig. S4 Pictures of aliquot solution samples taken at regular time intervals (from left to right) during the successive electrochemical oxidation (a) and reduction (b) of **1** in acetonitrile at 0 °C (E_{ox} = +1 V and E_{red} = 0 V, respectively).

Chemical redox procedures and spectroscopic measurements

The monooxidised and monoreduced species were obtained by addition of a 10.0 and 1.0 mM acetonitrile solution (0.1 mL) of bromine and hydrazine respectively, to a 1.0 mM acetonitrile solution of **1** and **2** (0.1 mL) at –40 °C. X-band EPR spectra (ν = 9.463 GHz) of frozen-matrix acetonitrile solutions were recorded under non-saturating conditions on a Bruker ER 200 D spectrometer equipped with a helium cryostat.

Static and dynamic magnetic properties

Variable-temperature (2–300 K) direct current (*dc*) magnetic susceptibility measurements under applied fields of 0.25 (T < 20 K) and 5.0 kOe (T > 20 K) and variable-field (0–50 kOe) magnetisation measurements in the temperature range of 2–10 K were carried out on crushed crystals of **1** with a Quantum Design SQUID magnetometer. The magnetic susceptibility data were corrected for the diamagnetism of the constituent atoms and the sample holder.

Variable-temperature (2–10 K) alternating current (*ac*) magnetic susceptibility measurements under ±5.0 Oe oscillating field at frequencies in the range of 0.1–10 kHz were carried out on crushed crystals of **1** and also on concentrated acetonitrile solutions (15 mM), both before and after successive electrochemical oxidation (E_{ox} = +1 V) and reduction (E_{red} = 0 V) at 0 °C, under different *dc* magnetic fields (H_{dc} = 1.0, 2.5 and 5.0 kOe in solid state and 2.5 kOe in solution) with a Quantum Design Physical Property Measurement System (PPMS). A quartz tube (8 cm height × 5 mm outer diameter with 0.5 mm wall thickness) filled with the concentrated acetonitrile solution (5 mm height) was employed to carry out ac magnetic measurements in solution. The quartz tube fits perfectly to the plastic straw typically used in the PPMS devices.

Table S3. Selected parameters from the least-squares fit of the *ac* magnetic data at different applied *dc* magnetic fields through two-phonon Raman plus temperature-independent one-phonon direct processes for **1** in solid state and solution (see text)

H_{dc}[a] (kOe)	C[b] (s^{-1} K^{-n})	n[b]	k[c] (s^{-1})
Solid state			
1.0	39000 ± 7000	1.87 ± 0.15	-----
2.5	15100 ± 900	1.68 ± 0.05	-----
5.0	1600 ± 600	2.45 ± 0.20	41000 ± 3000
Solution			
2.5	2000 ± 400	2.35 ± 0.11	2800 ± 2000

[a]Applied *dc* magnetic field. [b]The pre-exponential and exponential coefficients for the Raman mechanism [$\tau^{-1} = CT^n$], [c]Coefficient for the temperature-independent direct mechanism [$\tau^{-1} = k$].

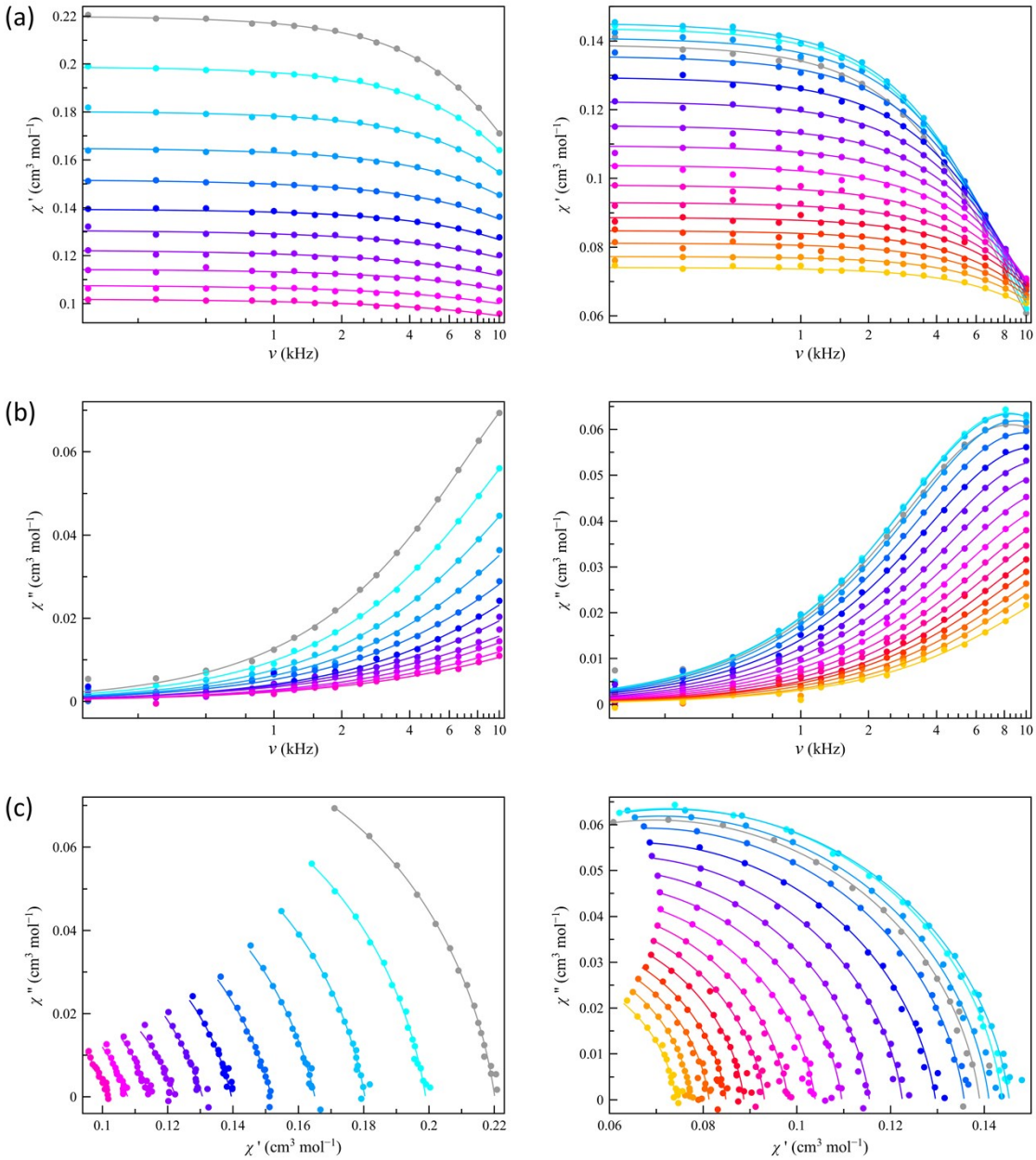

Fig. S5 Frequency dependence of χ_M' (a), χ_M'' (b), and the Argand plot (c) of **1** in the solid state and under static magnetic fields of 1.0 (left) and 5.0 kOe (right) with ±0.5 Oe oscillating field in the temperature range of 2.0–4.5 K and 2–6 K, respectively, in steps of 0.25 K (from grey to warmer colours). The solid lines are the best-fit curves simulated by using the values of χ_S, χ_T, τ and α shown in Figures 4 and S6.

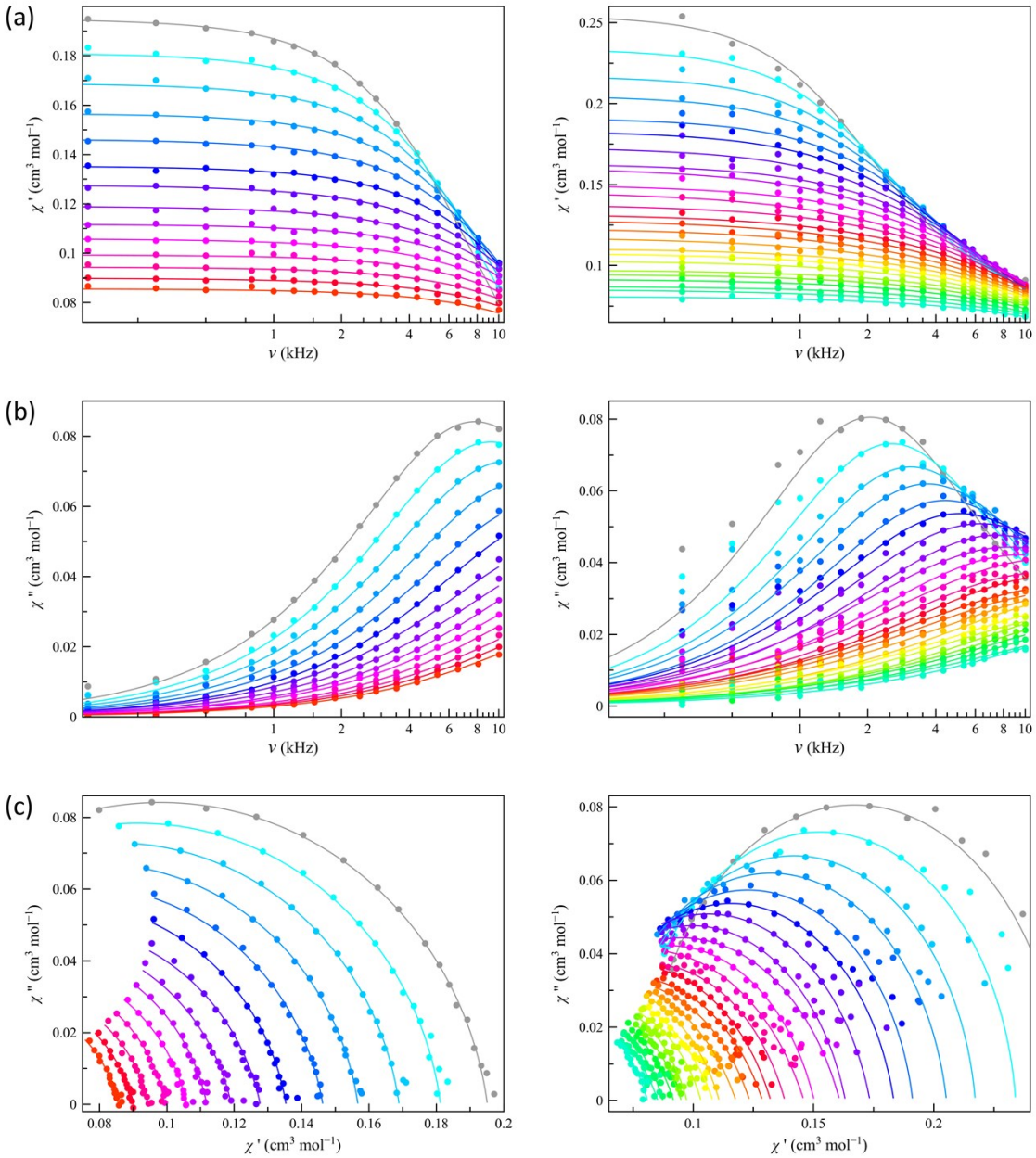

Fig. S6 Frequency dependence of χ_M' (a), χ_M'' (b), and the Argand plot (c) of **1** in solid state (left) and in solution (right) under a static magnetic field of 2.5 kOe with ±0.5 Oe oscillating field in the temperature range of 2.00–5.25 K and 2–8 K, respectively, in steps of 0.25 K (from grey to warmer colours). The solid lines are the best-fit curves simulated by using the values of χ_S, χ_T, τ and α shown in Figures 4 and S6.

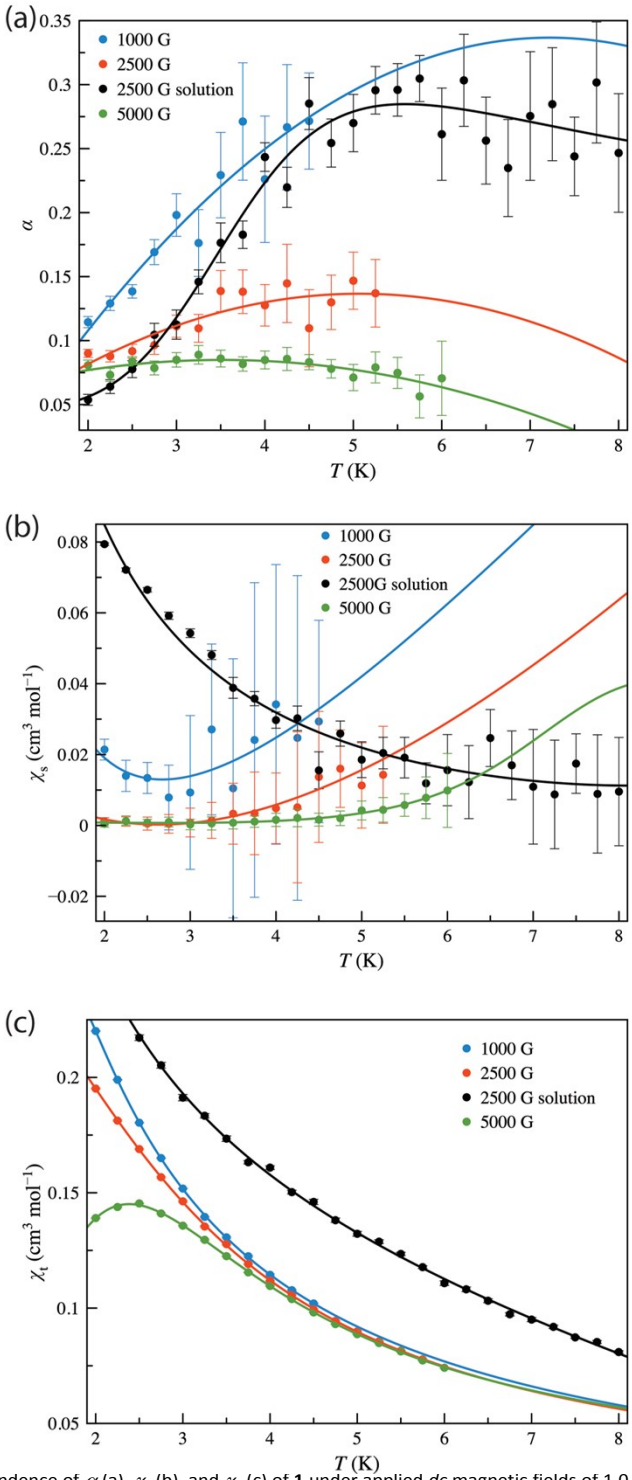

Fig. S7 Temperature dependence of α (a), χ_S (b), and χ_T (c) of **1** under applied *dc* magnetic fields of 1.0, 2.5, and 5.0 kOe in solid state and 2.5 kOe in solution. The solid lines are the best-fit curves for arbitrary equations. Standard deviations are given as vertical error bars.

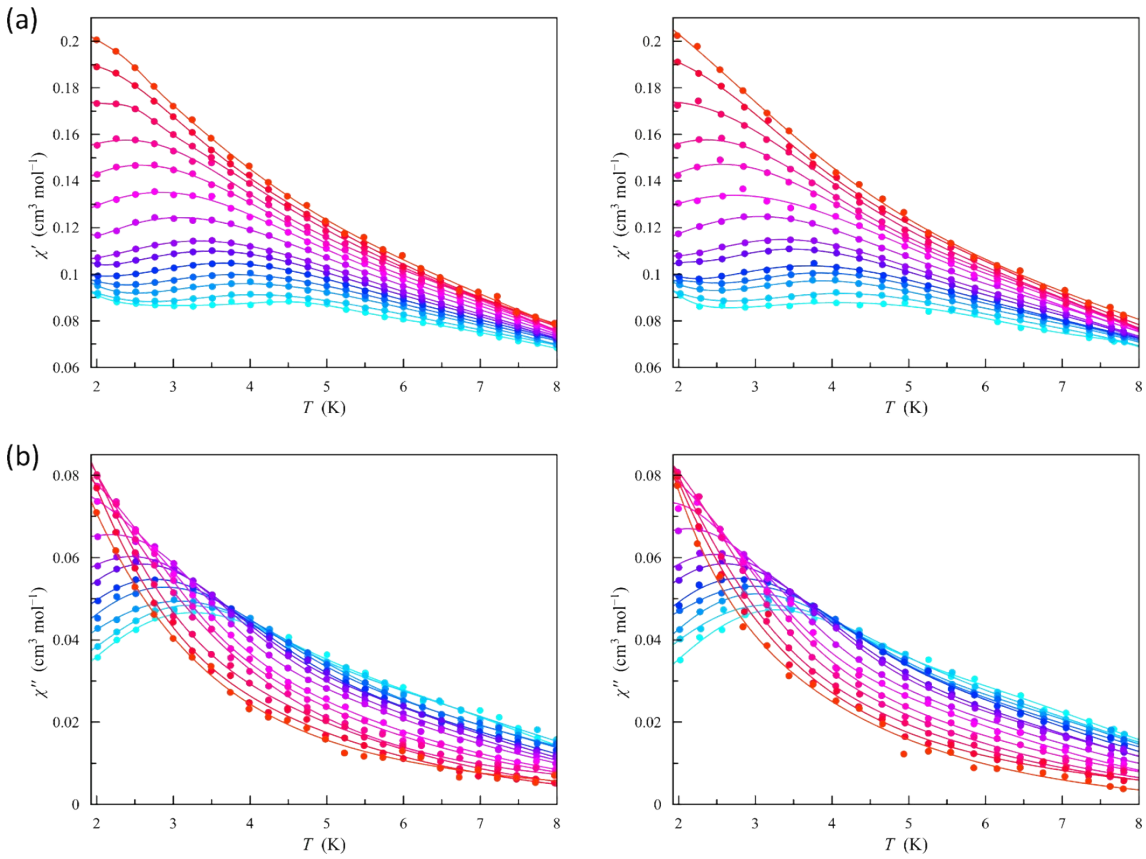

Fig. S8. Temperature dependence of χ_M' (a) and χ_M'' (b) of **1** in acetonitrile solution, either before (left) or after (right) one electrochemical redox cycle, at a ±5.0 G oscillating field in the frequency range of 1.23–10 kHz (from red to light blue), under an applied static magnetic field of 2.5 kOe. The solid lines are only eye-guides.